Fano resonance-based electrically reconfigurable add–drop filters in silicon microring resonator-coupled Mach–Zehnder interferometers

Linjie Zhou and Andrew W. Poon

Photonic Device Laboratory, Department of Electronic and Computer Engineering, The Hong Kong University of Science and Technology, Clear Water Bay, Hong Kong Special Administrative Region, China

Received August 14, 2006; revised December 15, 2006; accepted December 26, 2006; posted January 8, 2007 (Doc. ID 74028); published March 5, 2007

We report a Fano resonance-based electrically reconfigurable add–drop filter using a microring resonator-coupled Mach–Zehnder interferometer (MZI) on a silicon substrate. Our experiments reveal a pair of complementary Fano resonance line shapes that can be electrically tuned and output coupled from the MZI output ports. A near symmetrical resonance peak can be flipped to a near symmetrical resonance dip by applying a forward-bias voltage of less than 1 V across a laterally integrated p-i-n diode in the MZI non-resonator-coupled arm. Our scattering-matrix-based modeling shows good agreement with the experiments and indicates ways to enhance the resonance routing functionality. Our work demonstrates the feasibility of an integrated reconfigurable add–drop filter with actively interchangeable throughput and drop ports. © 2007 Optical Society of America

OCIS codes: 130.3120, 230.5750, 260.5740.

Reconfigurable optical add–drop filters are one of the building blocks in next-generation WDM optical networks. The recent development of silicon photonics that are largely leverage from the mature complementary metal-oxide semiconductor (CMOS) nanofabrication technologies makes it attractive to implement such reconfigurable add–drop filters using active microresonators on a silicon photonic chip.[1,2] Here we report the initial experimental demonstration of an electrically reconfigurable add–drop filter based on Fano resonance line–shape tuning in silicon microring resonator-coupled Mach–Zehnder interferometers (MZIs). The reconfiguration, characterized by interchanging the two complementary output-ports transmissions, is obtained through electrically tuning the relative phase between the MZI arms by applying a forward bias across a laterally integrated p-i-n diode as the MZI phase shifter.

Fano resonance,[3] resulting from interference between a resonance pathway and a coherent background pathway, is ubiquitous in various optical resonant configurations and nanophotonics devices.[4–7] The characteristic asymmetrical resonance line shapes can be varied by tuning the relative phase between the resonance and coherent background pathways. Recently, such line-shape tuning has been theoretically[8] and experimentally[9] investigated in MZI-coupled microresonators.

Figure 1 shows the schematic of a Fano resonance-based electrically reconfigurable add–drop filter on a chip. WDM channels (λ_1, λ_2, λ_3) launched into the integrated MZI input port (defined as the lower left port) is power split by the first 3 dB waveguide directional coupler. The MZI has two equal-length arms, with the upper waveguide coupled to a microring resonator (resonance wavelength λ_2) as a resonance pathway, and the lower waveguide laterally integrated with a p-i-n diode (enabling free-carrier-induced electro-optic phase shifts) as a background pathway. The two pathways are recombined by the second 3 dB waveguide directional coupler, and finally outcoupled to output ports 1 and 2. Without an induced phase shift at the background pathway ($\Delta\Phi=0$), λ_1 and λ_3 are transmitted to port 2 (throughput port), while channel λ_2 is dropped to port 1 (drop port), as shown in Fig. 1(a). With a $\Delta\Phi=\pi$ phase shift at the background pathway, the output–ports transmissions are interchanged, as shown in Fig. 1(b). In the case that λ_2 is launched from the add port instead (defined as the upper left port), then λ_2 is transmitted to port 2 with $\Delta\Phi=0$ and to port 1 with $\Delta\Phi=\pi$. Thus, by controlling the relative phase of the background pathway, we can reconfigure our add–drop filter by interchanging the throughput- and drop-port functionality.

We fabricate our devices on a silicon-on-insulator (SOI) substrate (0.21 μm device layer on a 2 μm buried oxide layer) using standard silicon microelectronics fabrication processes.[10] Figure 2(a) shows the top-view optical micrograph of a typical fabricated device. The MZI arm length is 1.2 mm to enable 2π

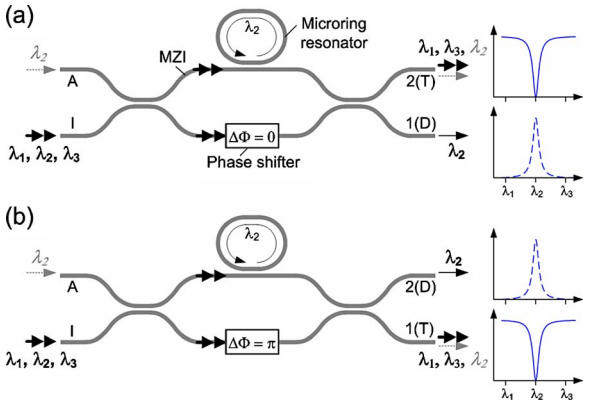

Fig. 1. (Color online) Schematic of the working principle of our reconfigurable add–drop filter under two conditions: (a) without phase shift ($\Delta\Phi=0$), and (b) with π phase shift ($\Delta\Phi=\pi$) of the nonresonance arm. I, input; T, throughput; D, drop; A, add. Schematic transmission spectra are shown.

0146-9592/07/070781-3/$15.00

phase tuning with a relatively small carrier-induced refractive index change. Two aluminum pads are connected to the laterally embedded 1.2 mm long p-i-n diode. Figure 2(b) shows the zoom-in view of the optical micrograph of the waveguide-coupled racetrack microring resonator. The microring curved waveguide radius is 25 μm. The lateral interaction length is 10 μm with a gap separation of 0.35 μm. Figure 2(c) shows the schematic cross-sectional view of the lateral p-i-n diode. The waveguide width is 0.4 μm with an etched depth of 0.18 μm. The n^+- and p^+-doped regions are 3 μm wide and have a separation of 0.5 μm from the waveguide sidewalls.

Figure 3(a) shows the measured TE-polarized (electric field parallel to the chip) transmission spectra for the two output ports without biasing the p-i-n diode. The port-2 transmission spectrum reveals a resonance $Q \sim 8000$ and an extinction ratio ~8 dB. Both port-1 and port-2 transmissions exhibit asymmetrical resonance line shapes, possibly due to fabrication-error-induced phase mismatch between the microresonator-coupled waveguide and the uncoupled waveguide. Figures 3(b)–3(e) show the measured TE-polarized output-ports transmission spectra with the p-i-n diode forward biased at V_d = 0.85 V, 0.89 V, 0.92 V, and 0.96 V, respectively. Fano resonance line shapes at different phases are discerned.

At V_d = 0.85 V, we observe a near symmetrical resonance peak at port-2 transmission and a near symmetrical resonance dip at port-1 transmission, with a peak-to-dip ratio (on–off ratio) of ~3.6 dB. Thus, the input resonance wavelength is preferentially dropped to port 2 acting as drop port, while other nonresonance wavelengths are preferentially transmitted to port 1 acting as throughput port. In contrast, at V_d = 0.92 V, port-1 transmission resonance line shape becomes a near symmetrical peak (acting as drop port), while port-2 transmission resonance line shape becomes a near symmetrical dip (acting as throughput port), with an on–off ratio of ~6.9 dB. The implication is that an input-coupled wavelength at a microring resonance can be controllably routed (add–drop) to either output port by a relatively small V_d change, and thus functioning as an electrically reconfigurable add–drop filter. We remark that although the asymmetrical resonance line shapes (e.g., V_d = 0.89 and 0.96 V) may not be directly utilized in the proposed reconfigurable add–drop filter applications, it is conceivable that the sharp asymmetrical line shapes can find applications in photonic signal processing and biosensing.[4–9]

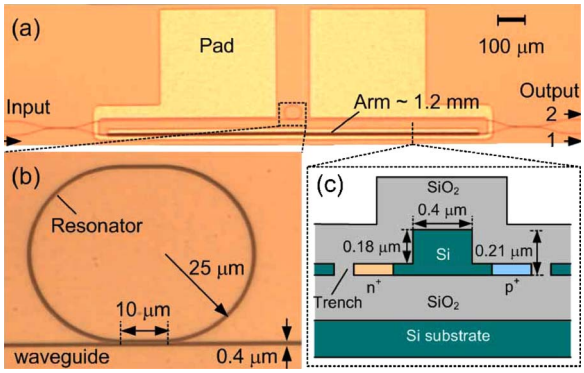

Fig. 2. (Color online) (a) Optical micrograph of the fabricated device. (b) Optical micrograph zoom-in view of the waveguide-coupled racetrack microresonator. (c) Schematic cross-sectional view of the p-i-n diode embedded in the nonresonance arm.

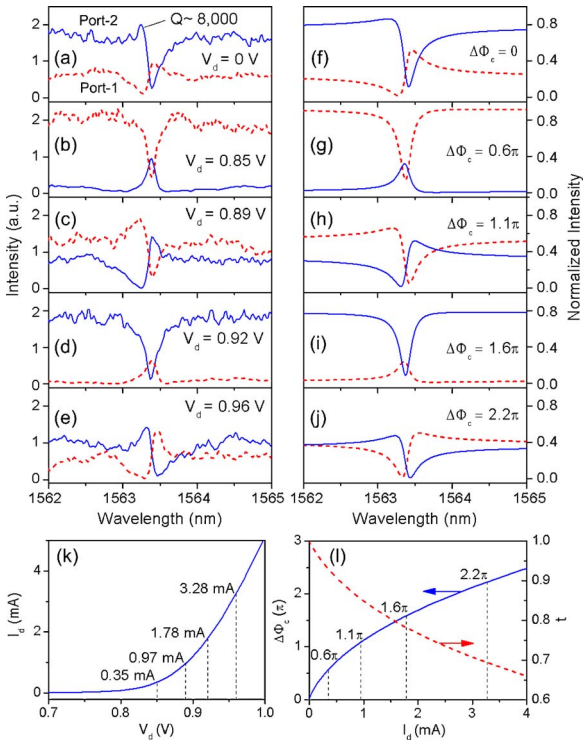

Fig. 3. (Color online) (a)–(e) Measured TE-polarized output-ports transmission spectra for the racetrack microring resonator-coupled MZI with various bias voltages. (f)–(j) Modeled corresponding output-ports transmission spectra. (k) Measured I-V curve of the embedded p-i-n diode. (l) Estimated current-induced phase shift $\Delta\Phi_c$ and transmission coefficient t in the nonresonance arm.

The gradual drop of the total transmitted optical power in ports 1 and 2 is due to the attenuated transmission in the nonresonance arm upon the increased free-carrier absorption loss. It should also be noted that our device insertion loss is considerably high at ~26 dB, comprising an estimated ~15 dB input-coupling loss and a measured ~20 dB/cm waveguide propagation loss (by cutback method), which exceeds the typical reported value of a few dB/cm loss for rib waveguides of similar dimensions.[11] We attribute the measured severe propagation losses to photolithography and dry-etching-induced sidewall roughness (can be mitigated using e-beam lithography and fine-tuned etching).

Using the free-carrier plasma dispersion and absorption formulas for silicon,[12] we estimate the free-carrier-induced refractive index and absorption coefficient variations Δn and $\Delta\alpha$ in the p-i-n diode intrinsic region based on the uniformly distributed free-carrier concentrations (simulated using MEDICI) at the four measured injection currents I_d [indicated by the dotted lines in Fig. 3(k)]. By using the beam-

propagation method, we obtain the wavelength-dependent waveguide effective refractive index n_{eff} and its free-carrier-induced variations Δn_{eff} and $\Delta\alpha_{\mathrm{eff}}$. Thus, the free-carrier-induced phase shift in the nonresonance arm is $\Delta\Phi_c=-\Delta n_{\mathrm{eff}}k_0L$, and the electric field transmission coefficient is $t=\exp(-\Delta\alpha_{\mathrm{eff}}L/2)$, where k_0 is the free space propagation constant and L is the MZI arm length. Figure 3(l) shows the $\Delta\Phi_c$ and t as a function of I_d at wavelength 1563.4 nm, indicating both phase shift and absorption loss (inversely proportional to $|t|^2$) increase with I_d.

We model our MZI-microresonator output-ports transmission spectra using the scattering-matrix approach. The output-ports electric field E_{o_1} (port 1) and E_{o_2} (port 2) are expressed as a function of the input- and add-port electric fields E_{in} and E_{ad} as follows:

$$\begin{pmatrix} E_{o_2} \\ E_{o_1} \end{pmatrix} = \begin{bmatrix} \cos(\theta_2) & -i\sin(\theta_2) \\ -i\sin(\theta_2) & \cos(\theta_2) \end{bmatrix} \times \begin{bmatrix} \left(\dfrac{\tau - Ae^{-i\phi}}{1-\tau Ae^{-i\phi}}\right)e^{-i\beta L} & 0 \\ 0 & te^{-i(\beta L-\Delta\Phi)} \end{bmatrix} \times \begin{bmatrix} \cos(\theta_1) & -i\sin(\theta_1) \\ -i\sin(\theta_1) & \cos(\theta_1) \end{bmatrix} \begin{pmatrix} E_{\mathrm{ad}} \\ E_{\mathrm{in}} \end{pmatrix}, \quad (1)$$

where θ_1 and θ_2 determine the power-coupling ratios of the directional couplers, τ is the light field transmission coefficient for the lightwave passing through the microresonator-coupled waveguide, A is the microring round-trip amplitude transmission factor, ϕ is the microring round-trip phase change, β is the propagation constant in the resonance arm and nonresonance arm (without free carriers), and $\Delta\Phi=(\Delta\Phi_0+\Delta\Phi_c)$ is the phase difference between the resonance arm and the nonresonance arm, comprising an initial phase mismatch $\Delta\Phi_0$ and a free-carrier-induced phase shift $\Delta\Phi_c$.

Assuming ideal 3 dB couplers ($\theta_1=\theta_2=\pi/4$) and light is only launched from the input-port ($E_{\mathrm{ad}}=0$), we express the input-normalized output-ports transmission intensities as

$$\frac{I_{o_1}}{I_{\mathrm{in}}} = \left|\frac{E_{o_1}}{E_{\mathrm{in}}}\right|^2 = \frac{1}{4}\left|-\left(\frac{\tau - Ae^{-i\phi}}{1-\tau Ae^{-i\phi}}\right) + te^{i\Delta\Phi}\right|^2, \quad (2)$$

$$\frac{I_{o_2}}{I_{\mathrm{in}}} = \left|\frac{E_{o_2}}{E_{\mathrm{in}}}\right|^2 = \frac{1}{4}\left|\left(\frac{\tau - Ae^{-i\phi}}{1-\tau Ae^{-i\phi}}\right) + te^{i\Delta\Phi}\right|^2. \quad (3)$$

From Eqs. (2) and (3), we see that I_{o_1} and I_{o_2} are swapped every π phase change of $\Delta\Phi$. In particular, when $\Delta\Phi$ equals even (odd) numbers of π, I_{o_1} shows a Lorentzian-like (inverted-Lorentzian-like) line shape and I_{o_2} shows an inverted-Lorentzian-like (Lorentzian-like) line shape, indicating the throughput or drop functionalities. Assuming light is only launched from the add port ($E_{\mathrm{in}}=0$), we can similarly deduce the corresponding add functionality.

We choose the estimated free-carrier-induced phase shifts [$\Delta\Phi_c=0$, 0.6π, 1.1π, 1.6π, and 2.2π; see Fig. 3(l)] for modeling the transmission spectra at port 1 and port 2. Figures 3(f)–3(j) show the modeled output-ports transmission resonance spectra (assuming $\Delta\Phi_0=0.32\pi$). Here we adopt $A=0.965$ and $\tau=0.95$, and find good agreement between the measured spectra [Figs. 3(a)–3(e)] and the modeled spectra.

Both our experiments and modeling results suggest relatively low on–off ratios between the resonance-peak and resonance-dip transmissions. We attribute the low on–off ratios to an imbalance between the microring loss and the coupling strength between the resonance arm and the microring. Our modeling also clearly indicates ways to enhance the on–off ratios. For example, by increasing the coupling strength with $\tau=0.9$, we expect a ~10 dB on–off ratio with an expense of Q (~5400). Alternatively, by reducing the microring loss with $A=0.982$, we also obtain an ~10 dB on–off ratio with an enhanced Q (~10,500). We caution that the two 3 dB directional couplers are essential or there is includible crosstalk between the throughput and drop-port transmissions for nonresonance wavelengths. Given its demonstrated ease of control on the resonance line shapes, our Fano resonance-based devices can function as, but not limited to, electrically reconfigurable channel add–drop filters for applications in WDM optical networks.

The research was supported by a grant from the Research Grants Council of the Hong Kong Special Administrative Region, China (project 618505). A. W. Poon's e-mail address is eeawpoon@ust.hk.

References

1. M. C. M. Lee and M. C. Wu, Opt. Lett. **31**, 2444 (2006).
2. E. J. Klein, D. H. Geuzebroek, H. Kelderman, G. Sengo, N. Baker, and A. Driessen, IEEE Photon. Technol. Lett. **17**, 2358 (2005).
3. U. Fano, Phys. Rev. **124**, 1866 (1961).
4. S. Fan, Appl. Phys. Lett. **80**, 908 (2002).
5. C. Y. Chao and L. J. Guo, Appl. Phys. Lett. **83**, 1527 (2003).
6. H. T. Lee and A. W. Poon, Opt. Lett. **29**, 5 (2004).
7. A. R. Cowan and J. F. Young, Phys. Rev. E **68**, 046606 (2003).
8. Y. Lu, J. Yao, X. Li, and P. Wang, Opt. Lett. **30**, 3069 (2005).
9. K. Y. Hon and A. W. Poon, in Laser Beam Control and Applications, Proc. SPIE **6101**, 61010V-1 (2006).
10. L. Zhou and A. W. Poon, Opt. Express **14**, 6851 (2006).
11. F. Xia, L. Sekaric, and Y. A. Vlasov, Opt. Express **14**, 3872 (2006).
12. R. A. Soref and B. R. Bennett, IEEE J. Quantum Electron. **23**, 123 (1987).